Final Report – AFOSR Nanoscience and Technology Initiative

Development of ultra sensitive nanoscale biosensor devices using carbon nanotube-field effect transistors (CNT- FETs)

July 27, 2005

Name of Principal Investigator: Asst. Prof. Hee Cheul Choi
e-mail address: choihc@postech.edu
Institution: Department of Chemistry, Pohang University of Science and Technology (POSTECH)
Mailing address: Department of Chemistry, POSTECH Pohang, San 31 790-784 Korea
Phone: 82-54-279-2130
FAX: 82-54-279-3399
Co-investigators (names and institutions):
Collaborators: Prof. Hongjie Dai (Sanford University, Chemistry), Prof. Chongwu Zhou (University of Southern California, Electrical Engineering), Prof. Joon Won Park (Pohang University of Science and Technology, Chemistry)

Abstract
Direct formation of iron phosphate nanoparticles on solid substrates with a narrow size distribution (average diameter = 2.2 nm) has been achieved by a simple spontaneous reaction of ferric chloride and phosphoric acid on hydroxyl-terminated SiO_2/Si substrates. Single-walled carbon nanotubes (SWNTs) are grown in high yield from the synthesized iron phosphate nanoparticles by thermal chemical vapor deposition (CVD) method as confirmed by AFM and Raman spectroscopy. Furthermore, three-terminal p-type nanotube network field effect transistor (FET) devices are successfully fabricated with the synthesized SWNTs using a conventional photolithography technique. The reduced solubility of Fe(III) ions when they form iron phosphate salts in aqueous media is the main driving force for the nanoparticle formation. Systematic control experiments have revealed that surface property, concentration and pH of the reaction solution equally play important roles the formation of nanoparticles.
As a second part of the projects, ultrasensitive nanotube FET devices have been developed by fabricating the devices using a shadow mask. A substantial increase of the sensitivity by more than five orders of magnitude has been achieved by increasing the area of active sensing region. While the nanotube FET devices fabricated by a conventional photolithography technique show their sensitivities at ~ 100 nM for general proteins, such as Streptavidin (SA) and Protein A (SpA), the devices made by using a shadow mask show typical sensitivities as low as ~ 1 pM. The increase of Schottky contact region formed at wider contact of metal electrodes and carbon nanotubes by a shadow mask metal evaporation as well as internal Schottky junctions of crossing multiple semiconducting and metallic carbon nanotubes are responsible for the increase of sensitivity.

I. Development of facile chemical routes for catalyst nanoparticles

Catalyst nanoparticles play a critical role for the formation of carbon nanotubes. Especially, size controlled catalyst nanoparticles are necessary in order to produce diameter controlled carbon

Report Documentation Page

Form Approved
OMB No. 0704-0188

1. REPORT DATE	2. REPORT TYPE	3. DATES COVERED
27 JUN 2006	**Final Report (Technical)**	**23-06-2004 to 26-05-2006**

4. TITLE AND SUBTITLE	5a. CONTRACT NUMBER
Development of ultra-sensitive nanoscale biosensor devices using carbon-nanotube field-effect transistors	**FA520904P0404**
	5b. GRANT NUMBER
	5c. PROGRAM ELEMENT NUMBER
6. AUTHOR(S)	5d. PROJECT NUMBER
	5e. TASK NUMBER
	5f. WORK UNIT NUMBER
7. PERFORMING ORGANIZATION NAME(S) AND ADDRESS(ES) **Pohang University of Science and Technology,San 31, Hyo-ja Dong,Pohang 790-784,NA,Korea**	8. PERFORMING ORGANIZATION REPORT NUMBER **AOARD-044065**
9. SPONSORING/MONITORING AGENCY NAME(S) AND ADDRESS(ES) **The US Resarch Labolatory, AOARD/AFOSR, Unit 45002, APO, AP, 96337-5002**	10. SPONSOR/MONITOR'S ACRONYM(S) **AOARD/AFOSR**
	11. SPONSOR/MONITOR'S REPORT NUMBER(S) **AOARD-044065**

12. DISTRIBUTION/AVAILABILITY STATEMENT

Approved for public release; distribution unlimited

13. SUPPLEMENTARY NOTES

14. ABSTRACT

Direct formation of iron phosphate nanoparticles on solid substrates with a narrow size distribution (average diameter = 2.2 nm) has been achieved by a simple spontaneous reaction of ferric chloride and phosphoric acid on hydroxyl-terminated SiO2/Si substrates. Single-walled carbon nanotubes (SWNTs) are grown in high yield from the synthesized iron phosphate nanoparticles by thermal chemical vapor deposition (CVD) method as confirmed by AFM and Raman spectroscopy. Furthermore, three-terminal p-type nanotube network field effect transistor (FET) devices are successfully fabricated with the synthesized SWNTs using a conventional photolithography technique. The reduced solubility of Fe(III) ions when they form iron phosphate salts in aqueous media is the main driving force for the nanoparticle formation. Systematic control experiments have revealed that surface property, concentration and pH of the reaction solution equally play important roles the formation of nanoparticles. As a second part of the projects, ultrasensitive nanotube FET devices have been developed by fabricating the devices using a shadow mask. A substantial increase of the sensitivity by more than five orders of magnitude has been achieved by increasing the area of active sensing region. While the nanotube FET devices fabricated by a conventional photolithography technique show their sensitivities at ~ 100 nM for general proteins, such as Streptavidin (SA) and Protein A (SpA), the devices made by using a shadow mask show typical sensitivities as low as ~ 1 pM. The increase of Schottky contact region formed at wider contact of metal electrodes and carbon nanotubes by a shadow mask metal evaporation as well as internal Schottky junctions of crossing multiple semiconducting and metallic carbon nanotubes are responsible for the increase of sensitivity

15. SUBJECT TERMS **Carbon nano tubes, Field-Effect Transistors, Biosensors**					
16. SECURITY CLASSIFICATION OF:			17. LIMITATION OF ABSTRACT	18. NUMBER OF PAGES	19a. NAME OF RESPONSIBLE PERSON
a. REPORT **unclassified**	b. ABSTRACT **unclassified**	c. THIS PAGE **unclassified**		**9**	

Standard Form 298 (Rev. 8-98)
Prescribed by ANSI Std Z39-18

nanotubes since the diameter of carbon nanotubes dictate the size of the nanoparticles. Although several chemical synthetic methods for the formation of uniform nanoparticles are reported, none of them is fully satisfactory. Most critically, the methods developed so far usually require complex apparatus with air sensitive precursor chemicals, and sometimes they utilize high-cost host molecules, such as dendrimer and ferritin. We have recently developed a facile chemical route for the formation of iron oxide nanoparticles using spontaneous clustering of Fe(III) ions with hydroxylamine. Although the exact mechanism is still unclear, spontaneous clustering of Fe(III) species seems to be accelerated by hydroxylamine on hydroxyl group terminated surfaces.
In the current project, we report our recent development of a facile room temperature chemical reaction for the formation of iron phosphate nanoparticles which are also excellent catalyst for the growth of diameter controlled single walled carbon nanotubes (SWNTs)

Spontaneous formation of iron phosphate nanoparticles on SiO_2/Si substrates is achieved by an immersion of pre-cleaned SiO_2/Si substrates into aqueous solutions containing ferric chloride and phosphoric acid (Figure 1(a)). Figure 1(b) shows a typical AFM image of spontaneously formed iron phosphate nanoparticles on SiO_2/Si at specific reaction condition which involves 200 µL of 10 mM phosphoric acid and 200 µL of 10 mM ferric chloride (pH of the final solution is 3.2). The reactions have been performed at room temperature and the reaction time is 3 min. For comparison, an AFM image of a bare SiO_2/Si substrate is shown as an inset.

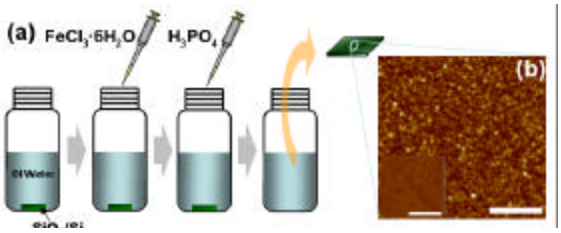

Figure 1. (a) A schematic of the reaction process, and (b) A typical AFM image of the produced iron phosphate nanoparticles

For the detail information about the size distribution of the prepared nanoparticles, 115 nanoparticles are selected from various regions and their diameters are individually measured from the height profiles using AFM (Figure 2). The histogram of the diameter distribution indicates that the average diameter is 2.2(8) nm. Although the total range of the diameters spans from 0.6 – 4.5 nm, more than 80% of the nanoparticles are found in the range of 1 - 3 nm. Considering the fact that there is no organic capping molecule involved, it is quite astonishing to obtain nanoparticles with such a narrow size distribution without severe aggregation.

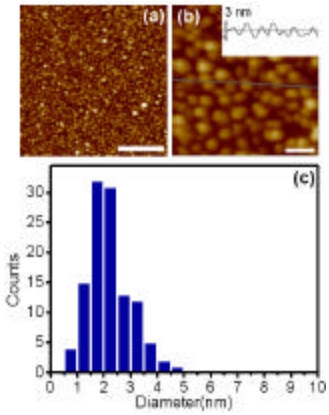

Figure 2. AFM images of spontaneously formed iron phosphate nanoparticles (a) in low magnification, and (b) in high magnification. (c) A histogram of size distribution of iron phosphate nanoparticles.

The major driving force for the nanoparticle formation is b ns in a The s .91 × 1 s that i on of v to be d cause surface

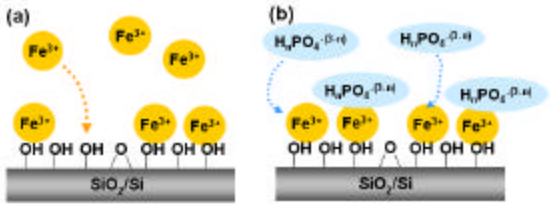

Figure 3. (a) Surface hydroxyl group mediated Fe(III) ion localization on the surface, and (b) cluster formation of iron phosphate

hydroxyl groups increase the local concentration of Fe(III) ions around the surface (Figure 3). In order to prove these hypotheses, we have systematically investigated the effects of surface property, concentration and pH of the reaction solutions on the formation of iron phosphate nanoparticles.

Effects of surface property on the iron phosphate nanoparticle formation: As a key factor for the nanoparticle formation, hydroxyl (-OH) groups on the surface play an important role. As shown in Figure 4(a), nanoparticles are formed in poor quality on the softly cleaned surfaces (only rinsed by copious amounts of DI water, acetone and IPA) where most of the surface hydroxyl groups may be hindered by various contaminants. However, Piranha treated surfaces show high quality nanoparticle formation in terms of population, size distribution and degree of aggregation (Figure 4(b)). In this case, Piranha treatment certainly helps to remove naturally stained organic residues almost completely, and consequently, maximizes the population of hydroxyl groups on the surfaces. We have further examined the substrates on which the population of hydroxyl groups is intentionally decreased by calcining them at 800 ? in air for 10 min.**Error! Bookmark not defined.** Indeed, low population of nanoparticles has been observed even after Piranha treatment (Figure 4(c)).

These results clearly show that the population of surface hydroxyl groups is critical for the determination of local concentration of Fe(III) ions near the surface, which directly affects the formation of water insoluble iron phosphate nanoparticles.

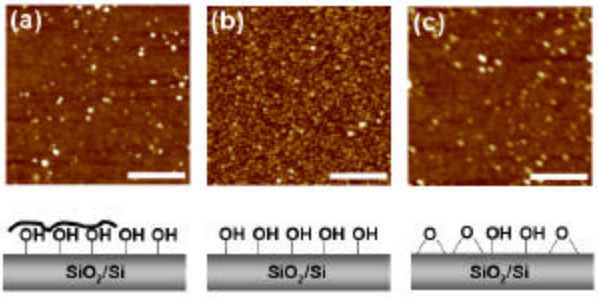

Figure 4. Iron phosphate nanoparticle formed on (a)softly-cleaned surface, (b) Piranha-cleaned surface, and (c) calcined surface at 800 °C in air.

Effects of concentration and pH on the iron phosphate nanoparticle formation: Dramatic c been observed when the concentrations o changed (Figure 5). Both sizes and p d when phosphoric acid concentration is i centration is fixed at 200 μM (Figures 5 concentration to 10 mM substantially d Next, when ferric chloride concentration is tion of phosphoric acid (200 μM), the p the concentration increase (Figures 5(g, d r increased to 4 mM, the number of n ar tendency is also observed when ferric c phosphoric acid concentration (4 mM, F

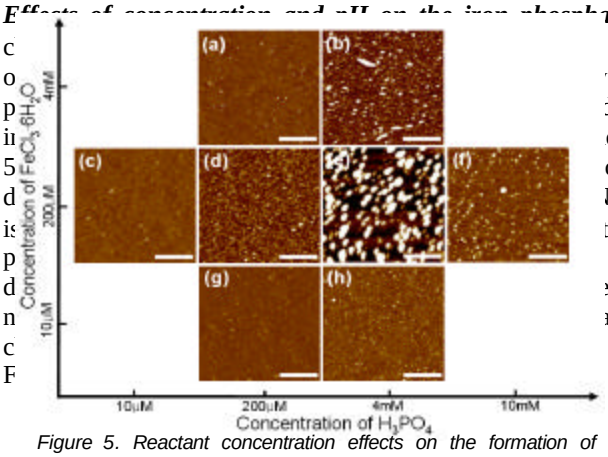

Figure 5. Reactant concentration effects on the formation of nanoparticles.

Since nonlinear dependence of nanoparticle formation on reactant concentration seems to be related with pH alteration of the solutions, we have further tested pH effects on the formation of nanoparticles.

Large variations in populations and size distributions of nanoparticles are observed when pHs of the solutions are varied from 2.1 to 10.7 (Figure 6). Interestingly, we have found that little or no particle has been formed at both extreme levels of pH. When 4 μmol of HCl is added into the original reaction solution (200 μM $FeCl_3$ + 200 μM H_3PO_4, natural pH = 3.2), pH drop is negligible (pH = 3.0), thus the population as well as the size of nanoparticles are almost identical (Figures 6(b) and (c)). When 80 μmol of HCl is further added, very few nanoparticles are formed with a significant pH drop (pH = 2.1, Figure 6(a)). Addition of 4 μmol of NaOH into the original solution increases the pH to 3.38 resulting in the aggregation of nanoparticles (Figure 6(d)). Further increase the pH to 10.7 yields almost no particle (Figure 6(e)).

At low pH, the dissociation constants of phosphoric acid ($K_{a1} = 7.52 \times 10^{-3}$, $K_{a2} = 6.23 \times 10^{-8}$, and $K_{a3} = 2.2 \times 10^{-13}$ at 25 ºC) are considerably decreased, hence the nanoparticle formation is suppressed due to the lack of available phosphate ions ($H_nPO_4^{(3-n)-}$, for n = 0, 1, 2). At high pH, on the other hand, the population of phosphate ion boosts up, so that the number of Fe(III) ions binding to a phosphate ion decreases to produce very small nanoparticles which are not even detectable by AFM[3].

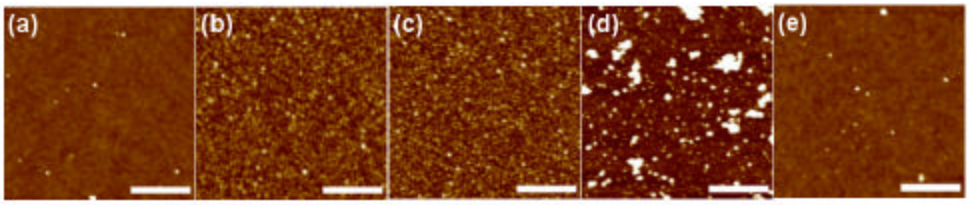

Figure 6. pH effects on the formation of iron phosphate nanoparticles. The pH of the solutions are (a) 2.14, (b) 3.00, (c) 3.21, (d) 3.38, and (e) 10.73.

X-ray photoelectron spectroscopic investigation: Figure 7 shows XPS spectra of the iron phosphate nanoparticles on SiO_2/Si substrate. All the spectra are internally calibrated with Au $4f_{7/2}$ peak from Au film that has been mounted with samples. In the survey spectrum, C 1s peak (284.6 eV) comes from residual impurities adsorbed on the surface when the sample is exposed to air, while the Si peak at 103.3 eV originates from the substrate. Since the nanoparticles form at a sub-monolayer level, the Fe and P peaks are relatively small compared to C, O or Si peaks. The detailed spectra of Fe and P region show that the binding energies of Fe $2p_{3/2}$ and P $2p_{3/2}$ are 712.5 eV and 133.4 eV, respectively. These results indicate that the binding energies of each element of the nanoparticles are almost identical to those of bulk iron phosphate (712.8 eV and 133.75 eV for Fe $2p_{3/2}$ and P $2p_{3/2}$, respectively)[4].

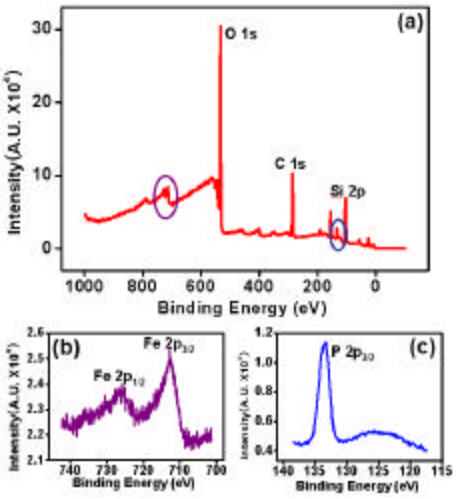

Figure 7. XPS spectra of the synthesized iron phosphate nanoparticles on SiO_2/Si substrates.

We have also tried to convert iron phosphate nanoparticles into iron phosphide (FeP) nanoparticles by reducing them in H_2 atmosphere under various elevated temperatures[5]. The conversion, however, is not successful as determined by XPS which fails to show any peak

shift of P $3p_{3/2}$ from iron phosphate. This might be because the removal of phosphorous as a form of phosphoric acid from iron phosphate nanoparticles is thermodynamically more favorable than the formation of iron phosphides in the reducing environment.

Synthesis of high yield single walled carbon nanotubes (SWNTs) and fabrication of nanotube network field effect transistors (FETs): Highly efficient catalytic activities of the spontaneously formed iron phosphate nanoparticles for the growth of SWNTs have been demonstrated. AFM studies show that SWNTs having 0.6 – 3 nm in diameters are successfully grown in high yield from iron phosphate nanoparticles on SiO_2/Si substrates by thermal CVD method (Figure 8(a)). Resonant micro Raman spectroscopy is also used to characterize average diameters of SWNTs at 3 μm of the spot radius. The diameters of SWNTs (d, in nm) are calculated from Raman shifts (ω_{RBM}, in cm^{-1}) of their radial breathing modes by the equation $\omega_{RBM}=248/d_t^6$. A typical Raman spectrum of SWNTs is shown in Figure 8(b). The six peaks in the region between 90 cm^{-1} and 250 cm^{-1} are identified as radial breathing modes and the peak at 1580 cm^{-1} as a G band which comes from in-plane graphene vibrational mode. For the diameter distribution statistics, 102 peaks taken from 50 different spots are investigated. As shown in Figure 8(d), the average diameter of carbon nanotubes is 1.5(4) nm and this value agrees well with 1.6(6) nm obtained by AFM measurements (Figure 8(c)).

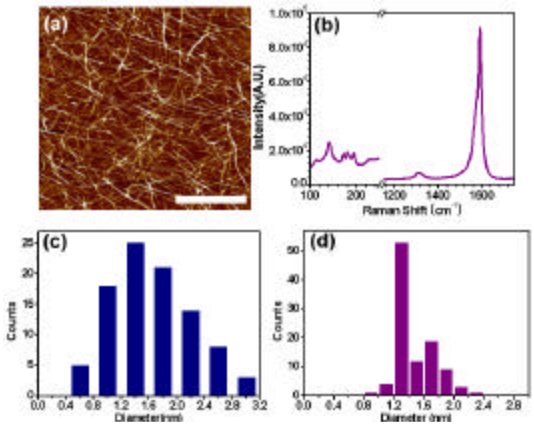

Figure 8. (a) AFM image of high yield SWNTs grown from iron phosphate nanoparticles using CVD. The scalebar is 1 mm. (b) A typical micro Raman spectrum of carbon nanotubes taken from (a). Histograms of size distribution obtained by (c) AFM height profiles (average diameter = 1.6(6) from 92 nanotubes) and by (d) micro Raman spectra (average diameter = 1.5(4) from 102 RBM peaks).

With high yield SWNTs grown from iron phosphate nanoparticles, we have also fabricated nanotube network FET devices by a conventional photolithographic technique. Figures 9(a) and (b) show a schematic and an optical image of a three-terminal FET device having multiple nanotube connections between the source and drain electrodes. A characteristic current vs gate voltage ($I-V_g$) curve of a p-type nanotube network FET device is measured by sweeping gate voltages from -10 to 10 V through Si back gate (Figure 9(c)). Although both metallic and semiconducting SWNTs coexist between the electrodes, the devices show more than 50% conductance changes by electrostatic gating at 10 mV bias (V_{ds}) due to the higher percentage of semiconducting SWNT population. This result is comparable to the previously reported data obtained from devices made of carbon nanotubes grown using Fe/Mo co-catalyst on alumina supporting catalysts[7]. One of the advantages using spontaneously formed iron phosphate nanoparticle catalyst over the alumina supported Fe/Mo catalyst is the absence of micron-sized supporting catalyst which has inability to control the diameters of nanotubes and causes problems for atomic scale investigation of carbon nanotubes, for example, with AFM.

Another characteristic feature of the nanotube network FET device is that SWNTs between two electrodes have web-like geometry, resulting in numerous quantum junctions, such as metallic-metallic, metallic-semicondcuting and semiconducting-semiconducting nanotube-nanotube junctions. Although most of the chemical sensing experiments using nanotube FETs currently focus only on nanotube-metal contact regions or surface of carbon nanotubes, systematic studies about these quantum junctions in nanotube network FET devices will provide great opportunities to develop more selective and sensitive sensor systems. Using the fabricated nanotube network FET devices, we are currently investigating the characteristics of internal Schottky junctions and their effects on sensing performance.

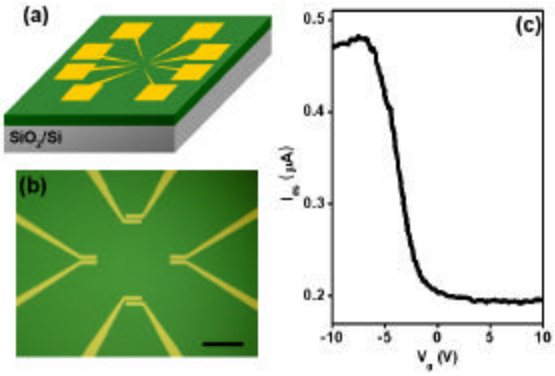

Figure 9. (a) A schematic view and (b) an optical microscope image of a p-type nanotube network FET device containing multiple SWNT connections between the source and drain electrodes. The scale bar is 200 ㎜. (c) A characteristic I-V_g curve obtained from a nanotube network FET device (V_{ds} = 10 mV).

II. Development of ultrasensitive SWNT-FET devices for protein sensing

Electrical sensing using one dimensional nanostructure based nanoscale electronic devices, such as carbon nanotube field effect transistors (SWNT-FETs), is one of the promising candidates for the detection of biomolecular events without labeling process involved. Other label-free biosensor systems have been also proposed to detect biospecific recognitions using surface plasmon resonance (SPR) and matrix assisted laser desorption/ionization (MALDI). However, electrical sensing systems have more advantages in term of easy access of outputs, real-time detection, and potential for future commercial applications as an integrated circuit form.

An important issue of SWNT-FET for biosensing application is sensitivity. Comparing to the conventional fluorescence based bioscreening method which generally shows picomolar (10^{-12} M) detection limit, SWNT-FET devices have reliable sensitivity at around hundreds of nanomolar (10^{-9} M) concentration level.[8] Success in the improvement for high sensitive SWNT-FET biosensors is closely related with the understanding of the sensing mechanism.

In the case of gas sensing, direct charge injection from electron withdrawing or donating molecules into the conduction bands of semiconducting carbon nanotubes causes conductance changes of the devices. However, we have recently found that the main reason of the conductance changes of SWNT-FET devices upon protein adsorption is Schottky barrier modulation at the contacts of metal electrodes and carbon nanotubes.[9] The work function changes of metal electrodes upon the adsorption of protein molecules induce the Schottky barrier height and thickness modulation, therefore resulting in the conductance changes at constant bias. This indicates that the sensitivity of SWNT-FET may be increased by providing larger Schottky contact area where more protein molecules can adsorb to induce conductance changes at lower concentration.

In order to increase Schottky contact area, SWNT-FET device is fabricated using a home-made Al shadow mask. Comparing to the devices fabricated by photolithography which provide small Schottky contact area, much thinner and wider Schottky contact area can be obtained by using a

shadow mask during the fabrication (Figure 10).

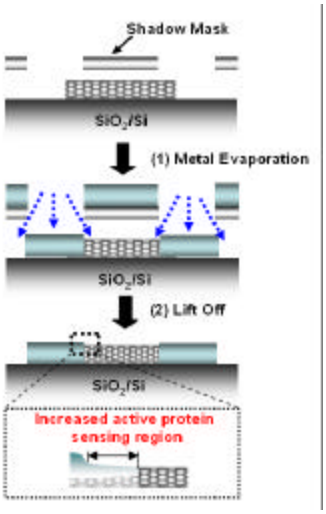

Figure 10. A schematic view representing fabrication of SWNT-FET devices using a shadow mask.

Fabrication of SWNT-FET devices using a shadow mask: We have first synthesized high yield SWNTs on SiO_2/Si by chemical vapor deposition (CVD) method. For the growth of SWNTs, iron containing catalyst nanoparticles were directly prepared on a SiO_2/Si substrate by an immersion of a pre-cleaned SiO_2/Si substrate into a scintillation vial containing 10 mL of DI water in which 10 μL of 10 mM ferric chloride ($FeCl_3$) and 100 μL of 10 mM hydroxylamine (NH_2OH) were sequentially added. After 3 min of reaction, the sample was thoroughly rinsed with DI water, then dried under N_2. This process was repeated three times in order to maximize the population of iron containing nanoparticles. Conversion of iron containing nanoparticles into iron oxide nanoparticle was performed by calcining it at 800? in air for 5 min. Note that the conversion of iron containing nanoparticles into iron oxide nanoparticles is not necessary for the growth of high yield SWNTs. The SiO_2/Si substrates containing catalyst nanoparticles were placed in the middle of an electric tube furnace equipped with gas flow controllers.

SWNTs were grown directly from the individual catalyst nanoparticles at 900? for 10 min under the gas flow of $H_2/CH_4/C_2H_4$ at the ratio of 1000/500/20 sccm. A simple resistance measurement for the SWNT grown substrates usually shows very low resistance (< 20 kohm). Figure 11(a) shows a typical AFM image of as grown SWNTs. On top of SWNTs, home-made Al strips with 500 μm width were placed to address source and drain electrodes by thermal metal evaporation of Cr (15 nm) followed by Au (30 nm). In order to exploit metal to spread under the shadow masks, the sample stage was tilted at 45° (Fig. 10).

The SWNT-FET devices fabricated by using a shadow mask typically show very low gate dependent conductivities. As shown in Fig. 11(b), the current drop of the device upon the Si back gate voltage sweep (I_{ds}-V_g) from -10 to 10 V is less than 15%. Considering that the similar devices fabricated by photolithography usually show more than 50% of current changes under the same gate voltage condition, the current device behaves like metallic nanotubes. This phenomenon is a direct signature indicating that the evaporated metals have been widely spread out under the shadow masks.

The sensitivity tests of the fabricated devices were performed in a home-built electrochemical cell in which 100 μL of PBS buffer (pH = 7.4) was filled. The source and drain electrodes were wired to a semiconductor analyzer (Keithley 4200 CS) using indium wires. The applied bias (V_{ds}) between the source and drain is 10 mV while the gate voltage was not applied.

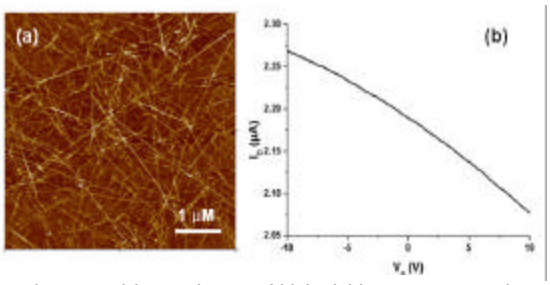

Figure 11. (a) AFM image of high yield SWNTs grown by CVD method, and (b) a typical I_{ds}-V_g curve of SWNT-FET devices fabricated by using a shadow mask, which show metallic transport behavior.

SA (Streptavidin) and SpA (Protein A) have been used to investigate nonspecific binding sensitivity of the devices. Figure 12 shows conductance changes upon the addition of SA at various concentrations. A significant conductance drop has been observed when 1 pM of SA is added. The conductance drop has been continuously observed until 1 nM of SA is added. The extents of conductance drop decreases as the concentration of SA increases, and this might be due to the saturation of the available sensing region. Similarly, SpA has also been detected at 1 pM concentration.

These results clearly show that the sensitivity of SWNT-FET devices has been improved by increasing metal-nanotube Schottky contact region. Along with the increased metal-nanotube Schottky contact region, there is another important characteristic features of the shadow mask-made SWNT-FET devices, which may assist to increase the sensitivity, i.e. internal junction Schottky contact. Because both semiconducting and metallic carbon nanotubes are simultaneously formed during the CVD growth, there will be many numbers of cross-junctions of semiconducting and metallic nanotubes, especially when nanotubes are grown in very high yield. Hence, these junctions build internal Schottky contacts and may facilitate the increase in sensitivity.[10]

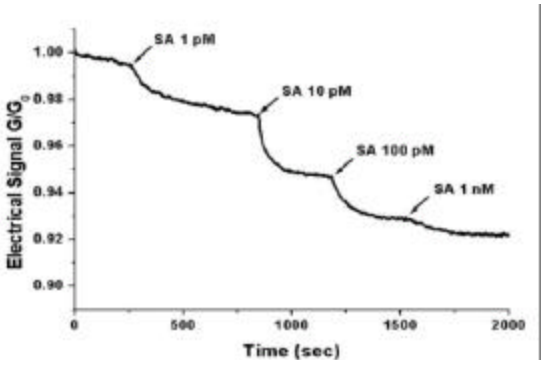

Figure 12. Conductance changes upon the nonspecific bindings of SA on the SWNT-FET devices fabricated using a shadow mask. (bias = 10 mV)

We are currently investigating the effects of internal Schottky contacts on protein sensing in detail by varying the distance between the source and drain electrodes, so that the number of internal Schottky contact can be controlled.

Summary

As a key component for the nanotube based electronic devices, we have developed an efficient and facile chemical route for the formation of iron phosphate catalyst nanoparticles by surface mediated spontaneous reaction. Highly pure SWNTs are grown in high yield using iron phosphate nanoparticles, which are further applied for the fabrication of nanotube network FET devices.

The SWNT-FET devices fabricated by using a shadow mask show substantially increased sensitivity for protein molecules. The increased metal-nanotube Schottky contact region that are achieved by evaporating metals under the shadow mask, accommodates much more protein molecules even at 1 pM concentration level to induce conductance change of the devices. Internal Schottky junction contacts formed by crossing semiconducting and metallic carbon nanotubes may also be responsible for the sensitivity improvement.

Publications

1. Hyun Jin Yang, Hyun Jae Song, Hyun-Jun Shin, Hee Cheul Choi "A rapid synthesis of iron phosphate nanoparticles via surface mediated spontaneous reaction for the growth of high yield single walled carbon nanotubes" *Langmuir*, **2005** (accepted)

2. Hye Ryung Byon, Hee Cheul Choi "Schottky contact engineering of carbon nanotube field effect transistor for ultrahigh sensitive biosensor application" **2005** (manuscript in preparation).

References

1. *CRC Handbook of Chemistry and Physics*, 85th Edition.
2. (a) Scaccia, S.; Carewska, M.; Bartolomeo, A.; Prosini, P. *Thermochimica Acta* **2002**, *383*, 145. (b) Gadgil, M. M.; Kulshreshtha, S. K. *J. Solid State Chem.* **1994**, *111*, 357.
3. At high pH, the local concentration of Fe(III) ions also diminishes due to the reduced electrostatic interaction between deprotonated Fe(III) hexaaquo-species (more negative) and surface hydroxyl groups (more negative).
4. NIST X-ray Photoelectron Spectroscopy Database, Version 3.4.
5. Stamm, K. L.; Garno, J. C.; Liu, G.. -y.; Brock, S. L. J. Am. Chem. Soc. ***2003***, 125, *4038*.
6. Jorio, A.; Saito, R.; Hafner, J. H.; Lieber, C. M.; Hunter, M.; McClure, T.; Dresselhaus, G.; Dresselhaus, M. S. *Phys. Rev. Lett.* **2001**, *86*, 1118-1121.
7. (a) Qi, P.; Vermesh, O.; Grecu, M.; Javey, A.; Wang, O.; Dai, H.; Peng, S.; Cho, K. J. *Nano Lett*. **2003**, *3*, 347. (b) Kong, J.; Soh, H. T.; Cassell, A. M.; Quate, C. F.; Dai, H. *Nature* **1998**, *395*, 878.
8. Chen, J. R.; Bangsaruntip, S.; Drouvalakis, K. A.; Kam, N. W. S. K.; Shim, M.; Li, Y.; Kim, W.; Utz, P. J.; Dai, H. *Proc. Natl. Acad. Sci*.. **2003**, *100*, 4984.
9. Chen, J. R.; Choi, H. C.; Bangsaruntip, S.; Yenilmez, E.; Tang, X.; Wang, Q.; Chang, Y. –L.; Dai, H. *JACS*. **2004**, *126*, 1563.
10. Fuhrer, M. S.; Nygård, j.; Shih, L.; Forero, M.; Yoon, Y. –G.; Mazzoni, M. S. C.; Choi, H. J.; Ihm, J.; Louie, S. G.; Zettl, A.; McEuen, P. L. *Science* **2000**, *288*, 494.